*Article*

# Rolling Shutter OFDM Scheme for Optical Camera Communication Considering Mobility Environment Based on Deep Learning

Huy Nguyen [ID], Van Linh Nguyen, Duc Hoang Tran and Yeong Min Jang *[ID]

Department of Electronics Engineering, Kookmin University, Seoul 02707, Korea
* Correspondence: yjang@kookmin.ac.kr; Tel.: +82-2-910-5068

**Abstract:** This paper presents a rolling shutter orthogonal frequency-division multiplexing (RS-OFDM) optical camera communication higher rate longer range proposed in IEEE 802.15.7a Task Group (TG7a) using an image sensor as a receiver. OFDM is a digital multi-carrier modulation scheme deployed for broadband wireless communication to resolve the inter-symbol interference (ISI) effect caused by the multipath channel. In optical wireless communication systems, OFDM was applied widely for indoor applications: internet of things, e-health, vehicular, and localization systems. The mobility scenario is a big problem for OWC systems, which reduces the system performance due to the optical channel variation in the processing time. In addition to that, signal detection should be considered in the mobility environment to improve the signal-to-noise ratio of OWC systems. In this paper, we proposed the convolution neural network (CNN) for LED detection in the RS-OFDM system, considering the mobility effect. In addition to that, the deep neural network was applied to detect the start of OFDM frame instead of conventional technology (Van De Beek algorithm). By applying our approach, the RS-OFDM system can achieve long communication (18 m distance) with a low error rate in the 2 m/s velocity environment.

**Keywords:** rolling shutter OFDM; RS-OFDM; deep learning for OCC system

## 1. Introduction

The demand for high-speed communication continues to grow, spurring technological innovations to boost efficiency and performance. Wireless communication outperforms wired communication because wireless communication is easier to set up and allows for ubiquitous data transmission without wires. Such innovations have proven crucial in the development of mobile networks. Radio frequencies (RFs) systems are gradually depleting their resources, necessitating the usage of a higher frequency range to boost data speed. Many researchers have been working on the millimeter-wave band to produce the fifth generation of mobile communications (5G), which has the potential to deliver a high data rate (1–10 Gbps). However, it is vital to highlight that the increased frequency can potentially have negative health consequences.

Visible light communication (VLC), light fidelity (LiFi), and optical camera communication (OCC) are new feasible candidates that could replace radio frequency communication. The advantages of VLC/LiFi/OCC compared with RF communication can be described as follows: If we provided the dimming and non-flicker technologies, light waves would have no harmful impact on human health. Ref. [1] shows that optical modulation frequencies up to 200 Hz can be considered without damaging human eyes. Visible light waves have a bandwidth more than 1000 times that of radio waves. Furthermore, visible light exists in light infrastructures on smart houses, hospitals, and automobiles, lowering the cost of adopting VLC/LiFi/OCC systems compared to the radio frequency systems.

Consequently, many businesses are devoting a significant portion of their budgets to studying this unique technology. IEEE 802.15 tutorials [2] provide an overview of the OWC

technology. The adoption of a wide range of protocol complexity and the peculiarity of OWC was also available in [2]. The IEEE 802.15.7 a Task Group (TG7 a) has divided the system into two categories:

- High rate OCC for IoT applications with four modulation schemes [3] considering mobility environment.
- High rate OCC for vehicular application with three modulation schemes [3] considering high mobility environment.

Contrasting VLC and Li-Fi systems, which use photodiodes to receive data, optical camera communication uses a camera as the detector. Refs. [4,5] show that the OCC system performance depends on the camera type. Global-shutter and rolling-shutter cameras are two types of cameras for this arrangement on the market. The camera frame rate, which decides whether the sampling rate meets the Nyquist sampling requirement, is the primary determinant of OCC performance with the global shutter camera. The rolling-shutter camera sampling rate is determined by both the camera frame rate and the camera's rolling rate.

OFDM (orthogonal frequency-division multiplexing) is a communication modulation technique for encoding digital data on multiple carrier frequencies. It is a useful approach in high data rate communication systems since the bandwidth is partitioned into orthogonal sub-carriers to reduce the distortion affected by inter-symbol interference (ISI). The sub-carriers in an OFDM system can overlap with other sub-carriers by utilizing the Fourier transform method without impacting signal performance. The cyclic-prefix was appended to compensate for the distortion to the OFDM symbol.

The camera on-off keying (C-OOK) system was introduced in paper [6], which can maintain a high data rate. IEEE 802.15.7–2018 standardized this method as well. On the other hand, the C-OOK system has several disadvantages, such as a high bit error rate (BER) and a short communication distance. In 2019, we suggested 2-D OFDM (2-dimention OFDM) based on screen code OCC in [7]. 2D-OFDM focuses on using asynchronous-quick-link (A-QL) code to collect the 2D-OFDM signal. The transmission distance of 2D-OFDM is a disadvantage, as it only operates reliably at 3 m [7]. MIMO C-OOK is based on the matched filter proposed in [8] with MIMO technique for high-rate OCC, but the mobility effect was not considered. We presented a rolling-shutter orthogonal frequency-division multiplexing (OFDM) technique for a high data-rate OCC system in [9]. Depending on the camera's rolling-shutter effect, the OFDM waveform could be received based on the LED intensity levels in each image. It reveals the drawback of the mobility effect, which is essential for OCC systems. In this paper, we propose an RS-OFDM, LED detecting method based on deep learning and the YOLOv5 algorithm to achieve high accuracy in real-time. With YOLOv5, we can achieve a low bit error rate with a mobility effect. In addition, a deep learning decoder presents a way to improve OCC performance as compared to the traditional [9] approach. By using deep learning for the start of frame detection, we can reduce the error in the mobile environment.

The remainder of this study contains five sections structured as follows. In Section 2, we present technical contributions. In Section 3, we represent the related work of OFDM techniques for OWC systems. Section 4 displays the system architecture of RS-OFDM using deep learning. Section 5 depicts the simulation and implementation results of the RS-OFDM system for the mobility environment. Section 6 concludes this study.

## 2. Technical Contributions

In this paper, we proposed a convolution neural network for LED detection and deep neural network for data decoding based on the RS-OFDM scheme considering mobility environment and long-range communication with low bit error rate. Some outstanding contributions of the proposed system can be represented as the following:

- The problem of complex noise (blur picture, interference, irregular attenuation) in an OCC system is difficult to tackle in the time domain, but it is simple to solve in the frequency domain by disregarding the DC component. The complex noise becomes

- more difficult in the mobility environment then; we need another algorithm to resolve this issue. Deep learning can help to reduce the noise effect.
- Mobility support: the RS-OFDM scheme based on the rolling-shutter effect revealed concerns for recognizing numerous LEDs since it was more sensitive to the mobility effect. While utilizing a rolling-shutter camera, the LEDs appeared in an image as black and white strips; when employing RoI algorithms, the number of LEDs could not be clearly recognized. As a result, we presented a neural network for increasing the OCC system's performance.
- By using deep learning for OFDM symbol detection, the bit error rate is reduced considering the mobility effect. As we mention below, the optical channel varies in the mobility environment, and then, the Van De Beek algorithm proved ineffective for RS-OFDM OCC system, especially the mobility environment. It is presented in Section 5. By collecting the real data from various cases (different distances, velocity, and exposure times), the input dataset was collected to train the deep learning model, which shows good performance compared to the conventional method we proposed in [9].

### 3. Related Works

In 1966, the Fourier transform (FT) was presented to the banks of sinusoidal frequency based on its orthogonality. To reduce the ISI effect, the cyclic-prefix (CP) was suggested in 1969 as an enhancement to OFDM systems. Researchers began to use OFDM for practical wireless communication in 1980. The FT is depicted in Equation (1).

$$X(\omega) = \sum_{i=-\infty}^{\infty} x[n]e^{-i\omega n} \tag{1}$$

Due to transmitting data by light source, the non-negative signal is a requirement in OWC signals. Then, before proceeding to the IDFT block, the waveform must be pre-processed. Asymmetrically clipped optical-OFDM (ACO-OFDM) and DC-biased optical-OFDM (DCO-OFDM) are currently two developed Li-Fi systems. On the other hand, the wavelet transform has several advantages over the Fourier transform, including no cyclic-prefix (CP) redundancy, reduced sub-channel interference, and greater spectral separation. The IEEE Standard Association recently defined wavelet OFDM (wavelet transform is the primary topic of IEEE 1901 for the power line communication (PLC)). It demonstrated that wavelet OFDM outperforms traditional OFDM. Ref. [10] proposes that wavelet OFDM is better than DCO-OFDM in terms of spectrum efficiency, side-lobe suppression, and bit error rate, and [11] proposes wavelet package approaches to OWC systems and shows that wavelet OFDM's PAPR (peak to average power ratio) is smaller and more robust in the face of channel imperfection. However, wavelet OFDM is difficult to deploy with high cost, so OFDM based on Fourier transform widely applied to the communication systems.

### 3.1. DCO-OFDM

DCO-OFDM is preferred more than ACO-OFDM for IM/DD techinues by some industrial companies and institutes, such as PureLiFi and Fraunhofer Heinrich Hertz Institute in Europe, as shown in [12,13], since the DCO-OFDM scheme provides better bandwidth efficiency when all subcarriers are used rather than just odd subcarriers. DCO-OFDM needs a post-processing step to guarantee that the light source waveform is unipolar. Adding DC-bias to generate a non-zero waveform within the LED operation range is the most accessible post-processing approach. Despite having a higher bandwidth efficiency, DCO-OFDM has a lower BER than ACO-OFDM because of the presence of DC bias.

Prior to arriving in the IDFT block, the OFDM signal $X = [X_0, X_1, X_2, \ldots, X_{N-1}]$, must be restricted to have Hermitian symmetry:

$$X_m = X_{N-m}^* \text{ for } 0 \leq m \leq \frac{N}{2} \text{ and } X_0 = X_{N/2} = 0 \tag{2}$$

With $m$ as the numerical order of OFDM elements and $N$ as the size of OFDM symbol. The signal $X$ is a real signal in the time domain after the IDFT block. The $k$th time-domain sample of $X$ is revealed:

$$x_k = \frac{1}{2} \sum_{m=0}^{N-1} X_m e^{\frac{j2\Pi.k.m}{N}} \tag{3}$$

The signal still has a negative component after this operation. The signal must then be DC-biased to ensure that it is non-complex and non-negative.

### 3.2. ACO-OFDM

The ACO-OFDM technique is frequently utilized in Li-Fi systems for photodiodes-equipment as receivers [14,15]. Different DCO-OFDM and ACO-OFDM only transmits over odd-subcarriers. In contrast, the BER performance of ACO-OFDM is more consistent than DCO-OFDM. The clipping noise spills into the detachable carriers on the receiving side because the null data was placed on even subcarriers, as seen in [16]. In ADO-OFDM, data symbols are carried on just the odd subcarriers to guarantee that the signal after the IDFT is non-complex and non-negative. The IDFT's input signal, $X$, consists solely of odd subcarriers $X = [0, X_1, 0, X_3, 0, \ldots, 0, X_{N-1}]$. The resulting real signal after the IDFT block is as follows:

$$x_k = -x_{k+\frac{N}{2}} \text{ for } 0 \leq k \leq \frac{N}{2} \tag{4}$$

With $k$ as the numerical order of OFDM elements and $N$ as the size of OFDM symbol.

## 4. System Architecture

### 4.1. Channel Coding

In digital communication systems, bit mistakes are found and fixed via a method called channel coding, commonly referred to as forward error correction coding (FEC). Both the transmitter and the receiver carry out channel coding. Channel coding is known as an encoder on the transmit side, where additional bits (parity bits) are added to the raw data before modulation. Due to noise, interference, and fading during transmission, channel coding enables the receiver to find and correct errors. In order to improve the OCC system performance, channel coding is employed in this paper as Figure 1.
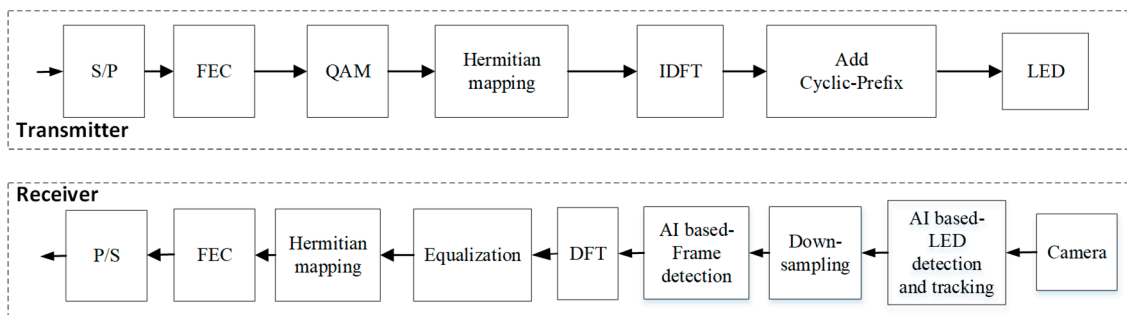


**Figure 1.** System Architecture.

### 4.2. Hermitian Mapping

The technological features of a rolling-OFDM system are presented in this section. Instead of putting the data symbol directly into the IDFT block, as in conventional OFDM in radio frequency, each symbol must transit via the Hermitian block. After that, the signal is routed into the IFFT. The Hermitian block provides the unique task of ensuring that the IDFT's output is completely real.

The Hermitian mapping process depicts in the equation below.

$$X_m = X^*_{N-m} \text{ for } 0 < m < N \text{ and } X_0, X_1, X_2 \ldots \ldots X_{N-1} \tag{5}$$

$$X = [0, X_1, X_2 \ldots \ldots 0 \ldots \ldots X^*_2, X^*_1] \tag{6}$$

### 4.3. Cyclic-Prefix (CP)

The cyclic-prefix (CP) is important in the OFDM system to mitigate inter-symbol interference. The length of CP is determined by the environment channel's symbol length and time delay. The cyclic prefix is generated by copying the bottom part of the OFDM symbol to the top of the OFDM symbol. Figure 2 shows the creation and insertion cyclic-prefix to the OFDM symbol.
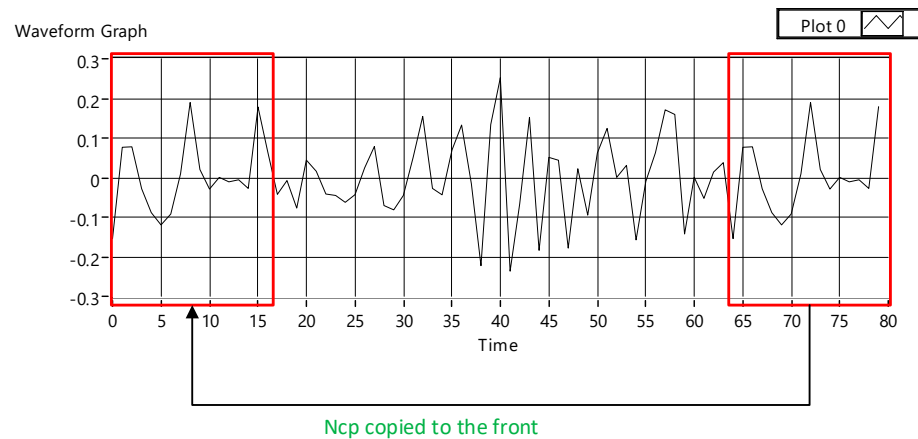


**Figure 2.** Cyclic-prefix in RS-OFDM symbols.

### 4.4. Pilot

Before transmitting, the pilots must add the signal to estimate the channel. A system's minimum pilot density and pilot position are critical. The pilot spacing used for the OFDM symbol was studied and implemented in [9].

Let $N$ be the OFDM symbol's length, $\Delta f$ be the spacing between subcarriers, and $N * \Delta f$ be the OFDM system's bandwidth.

Let $T_s$ be the spatial sampling period and $\tau$ be the time delay between spatial sampling. As indicated below, $\Delta p$ is the maximum pilot spacing:

$$\Delta p \leq \frac{N \Delta f}{2\tau/T_s} \tag{7}$$

The spacing between two adjacent pilots would be close for suitable interpolation performance. It should be emphasized, however, that the accuracy of the estimation is not proportional to the number of pilots. In circumstances where the channel is over-estimated, pilots placed too closely may compromise performance.

### 4.5. Deep Learning for LED Detection

In OCC system, RoI algorithms are well-established. Object and feature-based detection approaches are used in most RoI methods with real-time processing for object detection. As previously noted, with the rolling-shutter effect, LEDs are shown in images

represented by the intensity of LED strips corresponding to the OFDM waveform. Each image includes many strips, which make problems for RoI detection, particularly concerning the mobility effect. Deep learning neural networks are well-established methods for computer vision applications, e.g., object detection, image classification, localization, and image reconstruction. Convolution neural networks have emerged as promising candidates for deep learning-based computer vision applications. The CNN-based YOLO algorithm is a state-of-the-art, real-time object detection system. This paper proposes the customization and training of YOLO models for LED detection and tracking, considering the rolling-shutter and mobility effects.

To verify the performance of our approach, the experiment dataset was collected using real scenes. We recorded daytime and nighttime video footage with the mobility effect and generated 2500 blurry and clear images at different exposure times. Using these images as the dataset, we labeled images and trained the YOLOv5 model, which was modified with 5/7 convolution layers. Only one detection class was included. The corresponding number of filters in the final number of convolution layers was 38. The YOLOv5 model's average loss was about 0.09 after 10,000 training epochs with a low processing time of 0.0985 s for each epoch (NVIDIA GeForce GTX 1050).

### 4.6. Starting Point of OFDM Frame Detection

Van De Beek et al. suggested a time-frequency joint synchronization approach that uses CP to calculate a maximum likelihood function to predict the time and frequency deviation [17,18]. By utilizing the properties of cyclic-prefix, the start of OFDM frame may also be detected. In [9], we proposed the Van de Beek algorithm to detect the frame of RS-OFDM symbol in real-time for the OCC system. However, as we mentioned above, the mobility channel has a lot of effects on the OCC system (blur effect and SNR reduction, among others), so the conventional algorithm does not provide good performance for the RS-OFDM system. In this paper, we proposed deep learning for detecting the start of OFDM frame, as shown in Figure 3. We used a basic deep learning neural network model with two hidden layers to avoid overfitting the model. Following preamble detection, we can accurately detect the start of a frame of OFDM signals, improving the OCC system performance compared with matched filter technology in a mobility environment. In the case of overfitting, the accuracy of the test dataset is undermined when there are five or more hidden layers. The dataset was collected from several cases (different distances and velocities) with rolling shutter camera. The results of our proposed approach compared with the conventional scheme in [9] are shown in Section 5.
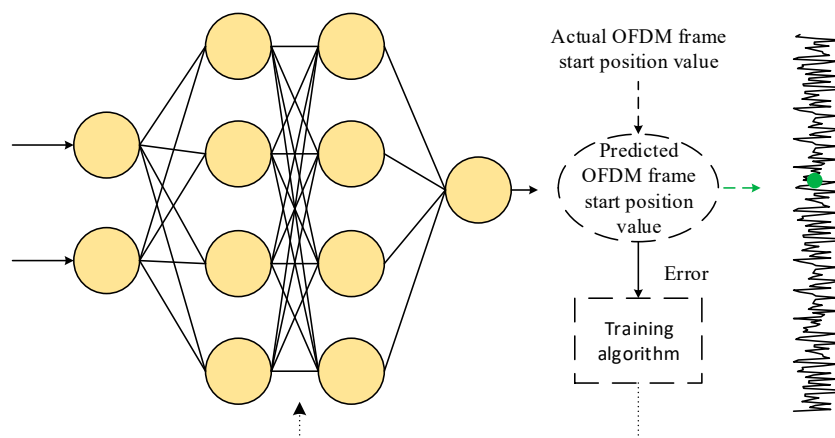


**Figure 3.** Deep learning for the starting point of OFDM frame.

### 4.7. Packet Structure

The format of the suggested scheme, as seen in Figure 4, is discussed in this section. Every packet can comprise numerous data sub-packets (DSs) to provide frame rate variation compatibility. Each sub-packet in the same packet contains the same payload with the

same sequence number (SN). The SN represents the serial number of packets. We may actually split two scenarios based on the transmitter's packet rate and the camera's frame rate. In the case of undersampling, the frame rate is lower than the transmitter's packet rate (LED). In the case of oversampling, the frame rate is many times higher than the transmitter's packet rate. The transmitter's packet rate is defined as the number of packets that carry distinct payloads across the transmission media in a certain time period (for example, 20 packets/s). Many data packet frames are included in our proposed data frame structure. Each data sub-packet (DS) contains payload data and an SN, and each packet is made up of numerous data sub-packets (DS). The SN denotes a data packet's sequence information, which aids a receiver in determining the arrival state of a new payload in the oversampling case and detecting lost payloads in the undersampling case. We can modify SN length depending on the OCC system parameters and optical channel. Then, the number of missing packets discovered grows as the SN length increases. Figure 5 illustrates how to apply SN to two common scenarios: oversampling and undersampling.
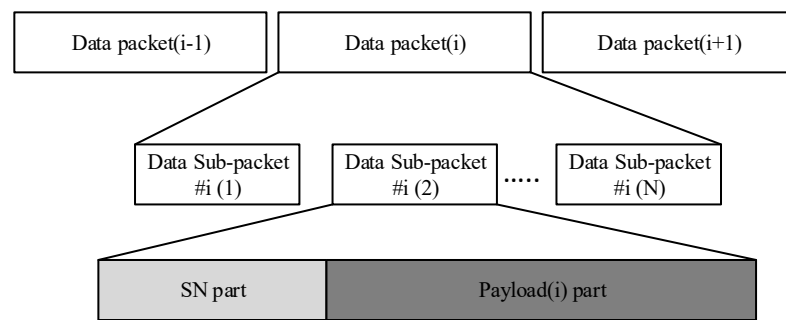


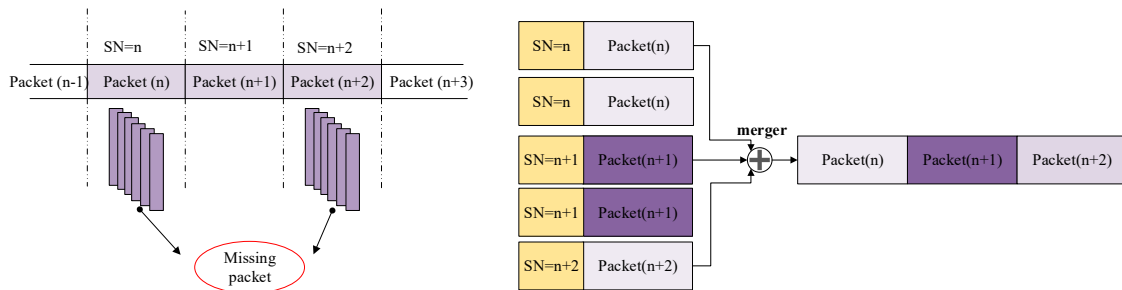**Figure 4.** The proposed data frame structure for RS-OFDM system.



**Figure 5.** Detection of lost packets and merging packet method using sequence number.

4.7.1. Undersampling

The undersampling case occurs if the frame rate drops below the transmitter's packet rate. The payload is lost in this case. Figure 5 depicts the use of the SN to detect a missed payload. The SN can identify the missed payload if the SN length is long enough. The SN is represented as n − 1 in the data frame obtained from the payload n − 1. The SN in the following data frame is n; however, the actual data frame has an SN of n + 1. The loss is identified by matching the SN of two adjacent data sub-packets, demonstrating that the payload n is missed. However, depending on the SN's length, a variety of states are formed. The sequence number, for example, can detect seven missing payloads of transmitted packets if the SN length is 3 bits. When problems are recognized, it is much easier to correct them. The mistakes occur when two successive packets have two non-consecutive SN (n − 1 and n + 1), as revealed in Figure 5.

### 4.7.2. Oversampling

When a rolling-shutter camera's frame rate exceeds (at least doubles) the transmitter's packet rate, every data packet is sampled at least twice (i.e., two pictures). We receive the same packet at the receiver, generating packet merger confusion. The SN is added to DS to assist the receiver in decreasing the influence of the camera's frame rate variation. Each packet contains identical DSs, which aids the receiver in removing superfluous data. When a DS is received, the receiver chooses which one has a compatible SN. As seen in Figure 5, the receiver side discards consecutive packets with the same SN and merges packets with successive SN (n − 1, n, n + 1).

## 5. Implementation Results

### 5.1. Estimation BER for Optical-OFDM Technologies

The symmetric clipping procedure in optical-orthogonal frequency-division multiplexing (O-OFDM) should be conducted in DCO-OFDM [19]. ACO-OFDM systems would also be used to reduce error in the bias cutting at the top of the OFDM signal.

We specified $K$ as the clipping process attenuation factor and $\beta_{bottom}$, $\beta_{top}$ as the top-cutting and bottom-cutting levels. We take the equation in [20,21]:

$$K = \frac{Cov(s, \psi(s))}{\sigma^2} = Q(\beta_{bottom}) - Q(\beta_{top}) \tag{8}$$

where *Cov[.]* denotes the covariance operator, $\sigma^2$ denotes the signal's variance, and $\psi(.)$ presents the normalized nonlinear transfer function.

The *BER* simulation of M-QAM O-OFDM is represented as:

$$BER = \frac{4(\sqrt{M}-1)}{\sqrt{M}\log_2(M)} Q(\sqrt{\frac{3\log_2(M)}{M-1}\Gamma_{b(elec)}}) + \frac{4(\sqrt{M}-2)}{\sqrt{M}.\log_2(M)} Q(3\sqrt{\frac{3\log_2(M)}{M-1}\Gamma_{b(elec)}}) \tag{9}$$

with $M$ is the number constellation of symbol QAM. In M-QAM DCO-OFDM, $\Gamma_{b(elec)}$ stands for receiver electrical SNR per bit on enabled subcarriers and is distinguished as follows:

$$\Gamma_{b(elec)} = \frac{K^2 P_{b(elec)}/G_B}{\sigma_{clip}^2 + \frac{G_B \sigma_{AWGN}^2}{g_{h(opt)}^2 G_{DC}}} = \frac{K^2}{\frac{G_B \sigma_{clip}^2}{P_{b(elec)}} + \frac{G_B \gamma_{b(elec)}^{-1}}{g_{h(opt)}^2 G_{DC}}} \tag{10}$$

where $\gamma_{b(elec)} = E_b/N_0$ is the electrical SNR in each bit; $\sigma_{clip}^2$ is the cutting noise variance; $G_{DC}$ is the attenuation of the electrical signal power; $g_{h(opt)}$ is the optical path gain coefficient; $G_B$ is the ratio of used for DCO-OFDM, $G = \frac{N-2}{N}$; and $N$ is the length of OFDM symbol. In addition to that, with ACO-OFDM, $G_B = 0.5$.

Figures 6 and 7 depict the estimated BER curves of ACO-OFDM and DCO-OFDM versus pixel $E_b/N_0$ with bottom- and top-cutting levels appropriate for the proposed scheme's deployed parameters. The figure shows that to attain a BER of O-OFDM schemes, the pixel $E_b/N_0$ must be at least 23 dB with DCO-OFDM and 18 dB with ACO-OFDM. The relationship between $E_b/N_0$ and *SNR* are as follows:

$$SNR = \frac{E_b}{N_0}\frac{R}{B} \tag{11}$$

where $R$ is the data rate of the OCC system (including error correction information and the other protocol overhead) and $B$ is the bandwidth of the OCC system. As previously stated, the pixel *SNR* values are be raised by selecting a longer exposure time, but this would restrict the communication bandwidth; therefore, communication bandwidth control must be carefully examined [22].
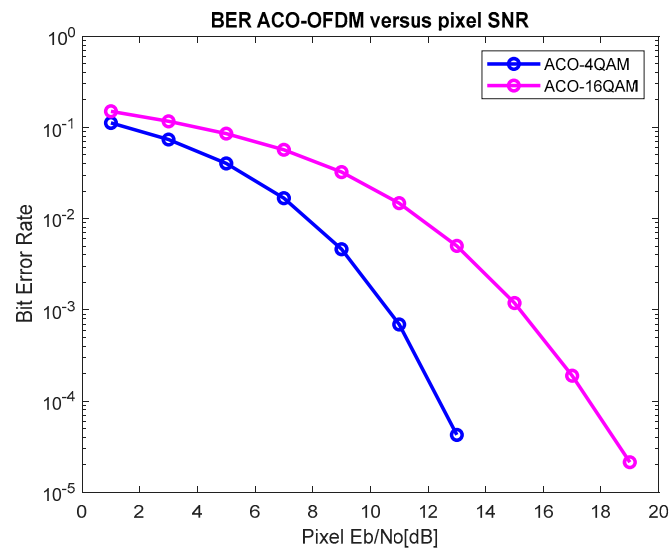
**Figure 6.** Simulation of BER ACO-OFDM versus pixel SNR.
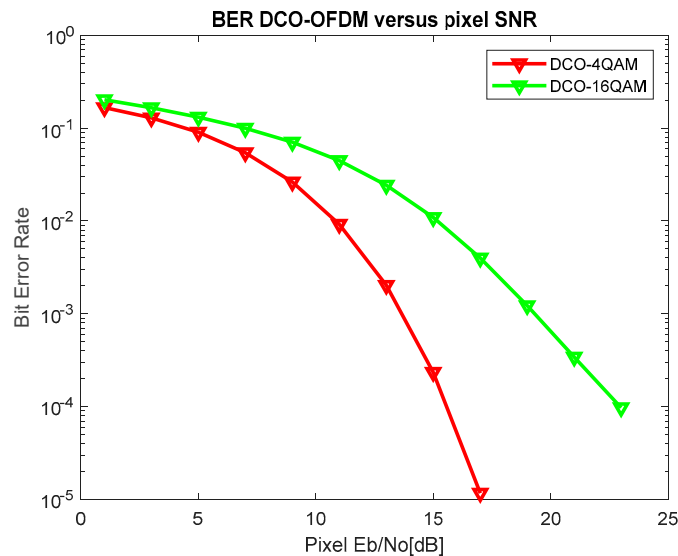


**Figure 7.** Simulation of BER DCO-OFDM versus pixel SNR.
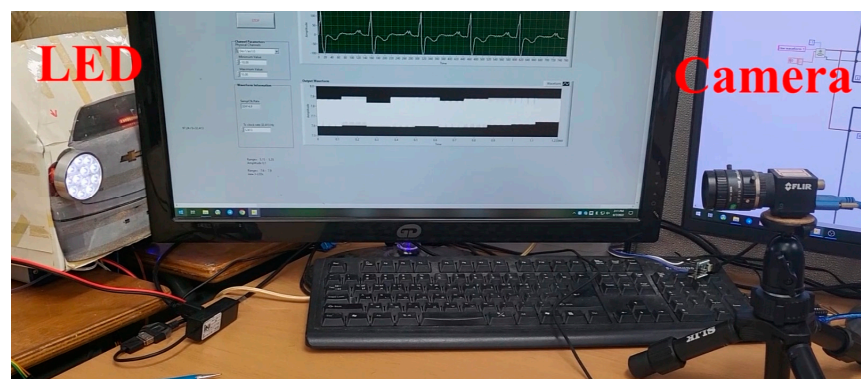
### 5.2. Implementation

Our studies with optical-OFDM schemes and various cameras have been repeated multiple times (different distances and exposure times) to demonstrate the frame variation effect. For the asynchronous procedure, the SN length was determined appropriately. Figure 5 depicts the architecture of a missing component and the data merging process. Table 1 also includes some experimental results and settings for OCC demonstration. The OFDM system was deployed with a PointGrey rolling-shutter camera with a frame rate variation of between 50 and 60 frames per second. The experimental setup is shown in Figure 8, and the OFDM waveform of the receiving camera is shown in Figure 9.

Table 1 displays the results of experiments carried out numerous times with varying optical clock rates. The data has been inserted into the asynchronous packet with the desired SN. The data merging and loss detection techniques are shown in Figure 5. In addition, the experimental results contain a variety of optical clock rates for various symbol lengths (128 bits and 256 bits) to assess the system's performance. The table demonstrates that if the symbol length is 128 bits, the data rate of 2.56 kbps is achieved, and the data rate of 5.12 kbps is achieved when the symbol length is 256 bits. As previously stated, the data

rate improves as the packet length increases; however, the trade-off between the image's LED size and the data rate must be carefully assessed [23].

**Table 1.** RS-OFDM parameters.

| Transmitter (LED 5 V, 4 W) | | |
|---|---|---|
| Clock Rate | 19.4 kHz | 43.4 kHz |
| OFDM length | 128 | 256 |
| FEC | Reed Solomon (15,11) | Reed Solomon (15,11) |
| Packet rate | 20 packets/s | 25 packets/s |
| Receiver | | |
| Camera | PointGrey rolling shutter camera | |
| Camera frame rate | 59 fps | |
| Data rate | | |
| Uncoded data rate | 2.56 kbps | 5.12 kbps |
| Coded data rate | 1.87 kbps | 3.75 kbps |



**Figure 8.** Scenario of RS-OFDM implementation.
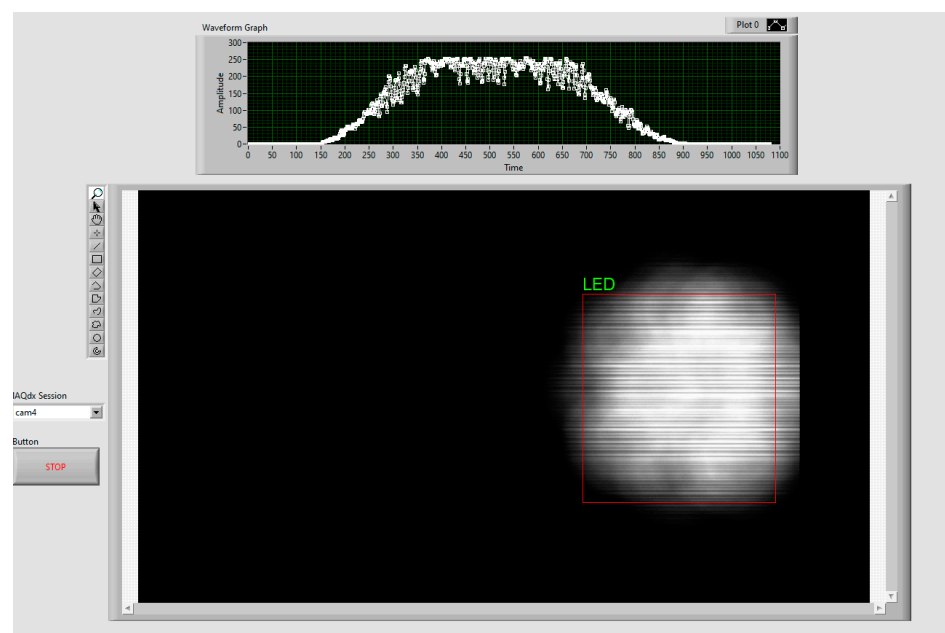


**Figure 9.** Rx interface.

Figure 10 displays the results of RS-OFDM schemes employing the Van De Beek algorithms and a deep learning neural network with varied distances at a 100 us exposure time (2–18 m). With a deep learning neural network, we can achieve BER of $10^{-5}$ at 2 m, while with the conventional scheme, we just achieve BER of $10^{-4}$. When the same distance and environment were used, the deep learning neural network decoder considerably enhanced the system's performance in the mobility environment over the conventional approach. For LED detection, a deep learning neural network was also used. It can also help with data decoding, which helps enhance performance for long communication distances and mobile contexts. In our implementation, we used a velocity of 2 m/s (walking velocity) to ensure that the proposed technique would suit indoor applications, considering the mobility effect. We implemented this scheme at a communication distance of 1 m, a visual representation of which is given in the Supplementary Materials section of this paper.
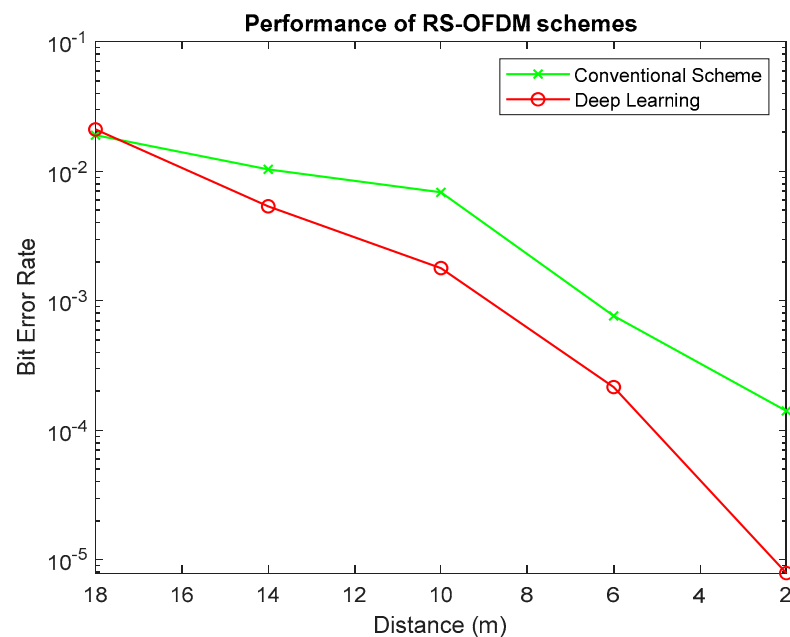


**Figure 10.** BER performance of RS-OFDM with deep learning and conventional schemes with velocity of 2 m/s.

## 6. Conclusions

This study proposed the RS-OFDM scheme for the mobility environment using a deep learning network. We applied deep learning algorithms not only for LED detection and tracking but also for decoding data. The YOLOv5 algorithm was deployed to detect multi-LEDs. With the rolling-shutter effect, the LED is displayed in images as black and white strips, which complicates clearly detecting LEDs compared with RoI detection. The comparison between deep learning and the conventional algorithm is revealed in this study. In addition to that, the packet structure of RS-OFDM was proposed to highlight the RS-OFDM system. Furthermore, a deep learning neural network for data decoding is helpful for long communication distances, particularly concerning the mobile environment. The measurement of the bit error rate of the RS-OFDM scheme using deep learning with different distances was provided compared with conventional. Based on our proposed approach, we can see that the BER can be reduced in the mobility environment.

**Supplementary Materials:** The following supporting information can be downloaded at: https://www.mdpi.com/article/10.3390/app12168269/s1. The supplementary material video shows the implementation of our proposal scheme at the distance of 1 m.

## References

1. Sridhar, R.; Richard, D.; Kyu, L.S. IEEE 802.15.7 Visible Light Communication: Modulation and Dimming Support. *IEEE Commun. Mag.* **2012**, *50*, 72–82.
2. Nikola, S.; Volker, J.; Min, J.Y.; John, L.Q. An Overview on High-Speed Optical Wireless/Light Communications. 2017. Available online: https://mentor.ieee.org/802.11/dcn/17/11-17-0962-02-00lc-an-overview-on-high-speed-optical-wireless-light-communications.pdf (accessed on 13 May 2022).
3. Nguyen, H.; Min Jang, Y. Draft D2-Merged Document for IEEE 802.15.7a TG. Available online: https://mentor.ieee.org/802.15/dcn/22/15-22-0234-02-007a-draft-d2-merged-document-for-ieee-802-15-7a-tg.docx (accessed on 13 May 2022).
4. Nguyen, H.; Min Jang, Y. Design of MIMO C-OOK using Matched filter for Optical Camera Communication System. In Proceedings of the 2021 International Conference on Artificial Intelligence in Information and Communication (ICAIIC), Jeju Island, Korea, 13–16 April 2021; pp. 474–476.
5. Nguyen, H.; Min Jang, Y. Design and Implementation of Rolling Shutter MIMO-OFDM scheme for Optical Camera Communication System. In Proceedings of the 2021 International Conference on Information and Communication (ICTC), Jeju Island, Korea, 20–22 October 2021; pp. 798–800.
6. Nguyen, T.; Islam, A.; Yamazato, T.; Min Jang, Y. Technical Issues on IEEE 802.15.7m Image Sensor Communication Standardization. *IEEE Commun. Mag.* **2018**, *56*, 213–218. [CrossRef]
7. Nguyen, T.; Hossain, M.A.; Jang, Y.M. Design and Implement of a Novel Compatible Encoding Scheme in the Time Domain for Image Sensor Communication. *Sens. J.* **2016**, *16*, 736. [CrossRef] [PubMed]
8. Nguyen, H.; Nguyen, V.; Nguyen, C.; Bui, V.; Jang, Y. Design and Implementation of 2D MIMO-Based Optical Camera Communication Using a Light-Emitting Diode Array for Long-Range Monitoring System. *Sensors* **2021**, *21*, 3023. [CrossRef] [PubMed]
9. Nguyen, V.H.; Thieu, M.D.; Nguyen, H.; Jang, Y.M. Design and Implementation of the MIMO–COOK Scheme Using an Image Sensor for Long-Range Communication. *Sensors* **2019**, *20*, 2258. [CrossRef] [PubMed]
10. Nguyen, H.; Thieu, M.D.; Nguyen, T.; Jang, Y.M. Rolling OFDM for Image Sensor Based Optical Wireless Communication. *IEEE Photonics J.* **2019**, *11*, 1–17. [CrossRef]
11. Hosseini, H.; Fisal, N.; Syed-Yusof, S.K. Wavelet Packet-based Multicarrier Modulation for Cognitive UWB Systems. *Signal Processing Int. J.* **2010**, *4*, 75–84.
12. Huang, W.; Gong, C.; Xu, Z. System and Waveform Design for Wavelet Packet Division Multiplexing-based Visible Light Communication. *J. Lightwave Technol.* **2015**, *33*, 3041–3051. [CrossRef]
13. Volker, J. *HHI High-Rate PD communication Proposal.* 2016. Available online: https://mentor.ieee.org/802.15/dcn/16/15-16-0016-03-007a-proposal-for-tg7r1-high-rate-pd-communications.docx (accessed on 13 May 2022).
14. Dobroslav, T.; Nikola, S. PureLiFi Low-Bandwidth PHY and MAC Proposal. 2016. Available online: https://mentor.ieee.org/802.15/dcn/16/15-16-0363-00-007a-text-input-lifi-low-bandwidth-phy-and-mac-d0.docx (accessed on 13 May 2022).
15. Zhou, J.; Wang, Q.; Cheng, Q.; Guo, M.; Lu, Y.; Yang, A.; Qiao, Y. Low-PAPR Layered/ Enhanced ACO-SCFDM for Optical Wireless Communications. *IEEE Photonics Technol. Lett.* **2018**, *30*, 165–168. [CrossRef]
16. Dissanayake, S.D.; Armstrong, J. Comparison of aco-ofdm, dco-ofdm and ado-ofdm in im/dd Systems. *J. Lightwave Technol.* **2013**, *31*, 1063–1072. [CrossRef]
17. Mondal MR, H.; Panta, K.R.; Armstrong, J. Performance of Two Dimensional Asymmetrically Clipped Optical OFDM. In Proceedings of the 2010 IEEE Globecom Workshops, Miami, FL, USA, 6–10 December.
18. van de Beek, J.J.; Sandell, M. ML estimation of time and frequency offset in OFDM systems. *IEEE Trans. Signal Process.* **1997**, *45*, 1800–1805. [CrossRef]

19. Edfors, O.; Sandell, M.; van de Beek, J.J.; Wilson, S.K.; Ola Borjesson, P. OFDM channel estimation by singular value decomposition. In Proceedings of the Vehicular Technology Conference—VTC, Atlanta, GA, USA, 28 April–1 May 1996.

20. Dimitrov, S.; Sinanovic, S.; Haas, H. A Comparison of OFDM based Modulation Schemes for OWC with Clipping Distortion. In Proceedings of the IEEE Workshop on Optical Wireless Communications, Houston, TX, USA, 5–9 December 2011.

21. Randel, S.; Breyer, F.; Lee, S.C.; Walewski, J.W. Advanced modulation schemes for short-range optical communications. *IEEE J. Sel. Top. Quantum Electron.* **2010**, *16*, 1280–1289. [CrossRef]

22. Dimitrov, S.; Sinanovic, S.; Haas, H. Clipping noise in OFDM based Optical Wireless Communication Systems. *IEEE Trans. Commun.* **2012**, *60*, 1072–1081. [CrossRef]

23. Nguyen, H.; Thieu, M.D.; Pham, T.L.; Nguyen, H.; Min Jang, Y. The Impact of Camera Parameters on Optical Camera Communication. In Proceedings of the 2019 International Conference on Artificial Intelligence in Information and Communication (ICAIIC), Okinawa, Japan, 11–13 February 2019.